

Transport of magnetically sensitive atoms in a magnetic environment

D.A. Kumpilov^{1,2}, I.A. Pyrkh^{1,2}, I.S. Cojocaru^{1,3,4}, P.V. Trofimova¹, V.A. Khlebnikov¹, P.A. Aksentsev^{1,4}, A.E. Rudnev^{1,2}, A.M. Ibrahimov^{1,2}, O.I. Blokhin^{1,2}, K.O. Frolov^{1,2}, S.A. Kuzmin^{1,2}, D.V. Gaifutdinov^{1,2}, A.K. Zyкова¹, D.A. Pershin^{1,3}, V.V. Tsyganok¹, A.V. Akimov^{1,3}

¹*Russian Quantum Center, Bolshoy Boulevard 30, building 1, Skolkovo, 143025, Russia*

²*Moscow Institute of Physics and Technology, Institutskii pereulok 9, Dolgoprudny, Moscow Region 141701, Russia*

³*PN Lebedev Institute RAS, Leninsky Prospekt 53, Moscow, 119991, Russia*

⁴*Bauman Moscow State Technical University, 2-nd Baumanskaya, 5, Moscow, 105005, Russia*

email: a.akimov@rqc.ru

Among interesting applications of cold atoms, quantum simulations attract a lot of attention. In this context, rare-earth ultracold atoms are particularly appealing for such simulators due to their numerous Fano-Feshbach resonances and magnetic dipole moments in the ground state. However, creating a quantum gas microscope with these atoms presents challenges, primarily because of the need to transfer the atoms from the main cooling chamber to another chamber with large optical access. Stray magnetic fields complicate this transfer by exerting forces on the atoms. Using thulium atoms as an example, the study demonstrates that stray magnetic fields can be measured directly using the atoms themselves, allowing for these fields to be accounted for during the transfer process. This approach significantly improves the efficiency of the transfer, allowing to transfer over 1/3 of the atoms from the main chamber to the scientific chamber, located 56 cm away.

I. INTRODUCTION

Rare-earth ultracold atoms are emerging as an intriguing platform for quantum simulations [1–8]. The presence of f -electrons causes a large magnetic moment in the ground state facilitating

long-range interactions [9,10], and a dense spectrum of low-field Feshbach resonances, providing detailed control over short-range interactions [11–15]. Moreover, rare-earth elements, so far, are the only cold atom platform, in which super solids have been observed [16–18].

A quantum gas microscope with ultracold atoms requires a high numerical aperture practically achieved by the creation of separate vacuum volumes [19–25]. There are a number of reasons, which make the transport of magnetic atoms complicated. First, the presence of an external magnetic field gradient causes an extra force, which affects the motion of the atoms. Next, the high density of Fano-Feshbach resonances typical of rare-earth atoms can cause losses of atoms when the magnetic field changes along the transport trajectory [11,12,15,26]. This situation requires high-precision control of the magnetic field during the entire trip of the atomic cloud. Finally, non-adiabatic changes in the magnetic field can cause depolarization of an atomic ensemble. All these reasons make the experimental calibration of the magnetic field extremely necessary.

A number of methods to transfer atoms between two vacuum chambers have been developed. One can use magnetic fields to transport atoms captured in magneto-optical traps (MOTs) [27,28]. In optical dipole traps (ODTs), transport is achieved using translation stages [29], focus-tunable lenses [30,31] and 1D optical lattices [32]. By transporting atoms in the ODT to the volume of the glass cell, a quantum microscope with non-magnetic ytterbium atoms was achieved [33].

This paper presents a method for reasonably fast optical transport of magnetic dipolar thulium atoms. This method exploits the maintenance of the magnetic field during the transport to preserve the polarization of the atoms at the lowest magnetic sublevel $|F = 4, m_F = -4\rangle$. Moreover, sophisticated tailoring of the focus-tunable waist position makes it possible to compensate for the force originating from the gradient of the magnetic field. This work paves the way for the development of quantum gas microscopes utilizing magnetic rare-earth elements.

II. EXPERIMENTAL SETUP

The precooling and trapping stages of the experiment closely followed procedures presented in previous studies [34–39]. The pre-cooling of the atoms was realized via the Zeeman slower and 2D optical molasses operated at the strong transition

$4f^{13}({}^2F^0)6s^2 \rightarrow 4f^{12}({}^3H_5)5d_{3/2}6s^2$ with a wavelength of 410.6 nm and a natural width of $\Gamma = 2\pi\gamma = 2\pi \cdot 10.5 \text{ MHz}$. Following the precooling stage, atoms were loaded into the MOT operating at the weaker transition $4f^{13}({}^2F^o)6s^2 \rightarrow 4f^{12}({}^3H_6)5d_{5/2}6s^2$ with a wavelength of 530.7 nm and a natural width of $\Gamma = 2\pi\gamma = 2\pi \cdot 345.5 \text{ kHz}$. Then the reduction of MOT light intensity provided the polarization of atoms at the lowest magnetic sublevel $|F=4; m_F=-4\rangle$ of the ground state [40–44]. The atoms were cooled down to $22.5 \pm 2.5 \text{ } \mu\text{K}$ and then loaded into the ODT formed by a linearly polarized laser beam waist of $30 \text{ } \mu\text{m}$ with a wavelength of 1064 nm.

The main chamber was formed in the Kimball Physics MCF800-ExtOct-G2C8A16 UHV vacuum chamber. The scientific chamber was formed by the Kimball Physics MCF133-SphCube-A6 UHV vacuum chamber with viewports on 5 sides of it, thus allowing the detection of an atomic cloud once it reaches the volume. The distance between the centers of the two chambers was measured at 55.6 cm. To implement the optical transport, the beam waist of a 1064 nm laser was created by a system of a focus-tunable lens and a plano-convex lens (Figure 1a). Variations of the optical power of the focus-tunable lens made it possible to alter the ODT beam waist position by more than 50 cm (Figure 1b) exceeding the distance between the main chamber and the science chamber. Theoretically, it is possible to maintain the constant beam waste on the entire atom transfer distance in the scheme demonstrated in Figure 1a. Practically, nevertheless, with 1-inch optics, the beam starts to clip at about halfway of the transfer. To avoid this clipping, the authors slightly misaligned the lenses, so that there was no clipping of the beam, but the waist slightly varied in size during transfer, changing from 30 to $44 \text{ } \mu\text{m}$ for the initial and final points of the optical transport (Figure 1c). It should be noted that this was not essential, and the waist diameter could also be fixed with larger aperture optics.

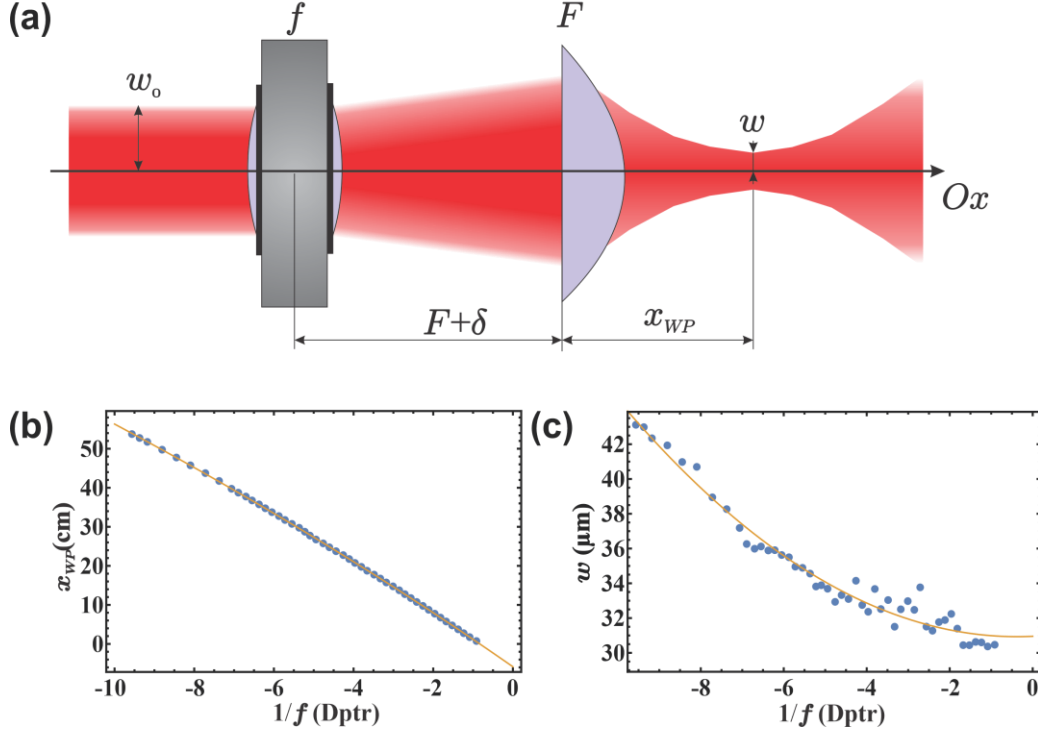


Figure 1. a) Optical scheme of the transport ODT. b) Waist coordinate versus the optical power of the tunable lens. c) Waist of the ODT versus the optical power of the tunable lens.

III. MAGNETIC FIELD MEASUREMENT

The atoms inside the ODT are subjected to the dipole force pushing them to the point with maximal intensity. Shifting the focus of the ODT beam forces the atoms to move along the beam axis. The main purpose of the transport is to maintain the polarization of thulium atoms on the lowest magnetic sublevel. Unfortunately, all the issues listed in the introduction are present for the thulium atom and need to be addressed. First, previous results revealed a remarkable depolarization in a low magnetic field [45]. To obtain a threshold magnetic field sufficiently suppressing the depolarization, the average polarization m_F was calculated via the Boltzmann formula:

$$\langle m_F \rangle = \frac{1}{Z(B)} \sum_{m_F=-4}^{m_F=4} m_F \text{Exp} \left[-\frac{m_F \mu_B g B}{k_B T} \right], \quad Z(B) = \sum_{m_F=-4}^{m_F=4} \text{Exp} \left[-\frac{m_F \mu_B g B}{k_B T} \right], \quad (1)$$

where B is the magnetic field absolute value, T is the temperature of the atomic cloud, and g is the Lande factor. For $T < 50 \mu\text{K}$ and $m_F < -3.95$, the value of B should exceed 2.27 G (Figure 2).

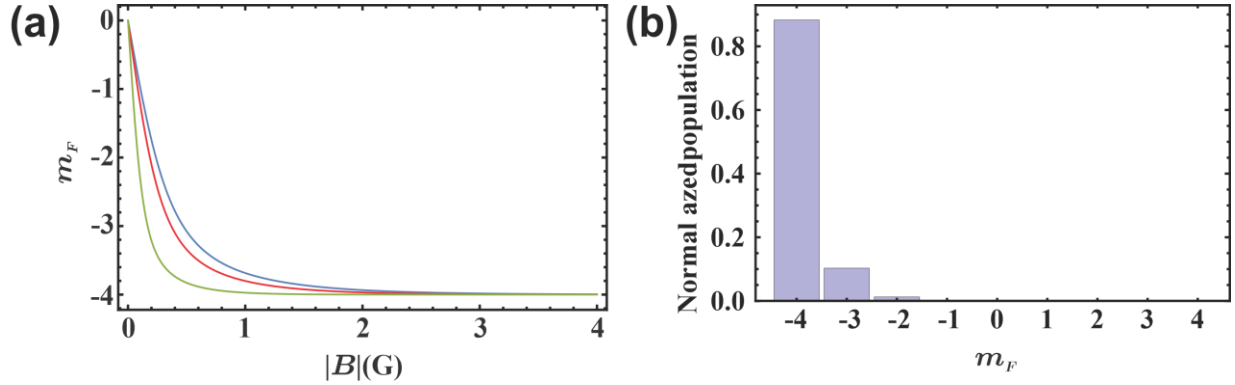


Figure 2. a) Average polarization of the cloud versus holding magnetic field for the green line $20 \mu\text{K}$, red line $40 \mu\text{K}$, and blue line $50 \mu\text{K}$. b) Normalized population of each m_F at holding a magnetic field of 1.2 G with a temperature of $40 \mu\text{K}$.

Second, the presence of Feshbach resonances imposes another restriction on the value of the magnetic field. Knowing the resonances spectrum for corresponding temperatures from work [11] and taking into account depolarization, the authors decided to maintain the magnetic field in the region of 3.65–3.95 G free of resonances.

Finally, magnetic field forces may affect the motion of atoms during transfer. Unfortunately, avoiding magnetic forces and steering away from Feshbach resonances require different approaches: the former is sensitive to the magnetic field gradient, while the latter is sensitive to the magnetic field value. The value of the magnetic field may be maintained by additional coils, the current of which is synchronized with the atomic motion. Such an approach requires the knowledge of the magnetic field along the transport trajectory.

The magnetic field was first calculated using the finite element method in the CST Studio Suite 2023. To find the spatial distribution of the magnetic field, one must know the magnetic properties of vacuum components. Most of them are made from 316L stainless steel, which has a magnetic permeability close to 1. However, the viewports on the main chamber in this study had braze sealings between flanges and glass. The braze material was highly ferromagnetic with unknown properties. They were measured with a DRV425 fluxgate magnetic-field sensor on a specially assembled stand. The stand was comprised of two rectangular coils in the Helmholtz configuration, which provided the uniformity of the magnetic field in the center of

the coils where the viewport was placed. The simulated magnetic field curve is shown in Figure 3b.

To verify the simulated results, the following experiment was conducted. The atoms were transferred to the point x_{WP} , where a 200-ms pulse of 530.7 nm resonance laser radiation illuminated the atoms and then they were returned to the main vacuum chamber where the imaging was performed (see Figure 3a).

The frequency of the 530.7 nm laser beam was scanned using an acousto-optic modulator around the transition frequency. Scanning the frequency of elliptically polarized green light along with subsequent imaging provides the resonance picture where one can determine two transitions $|F = 4, m_F = -4\rangle \rightarrow |F = 5, m_F = -4\rangle$ (π -transition) and $|F = 4, m_F = -4\rangle \rightarrow |F = 5, m_F = -3\rangle$ (σ^+ -transition) (see Figure 3c). The spacing between the two resonances is determined by the absolute value of the magnetic field B in the region near x_{WP} according to the relation

$$\nu(|4, -4\rangle \rightarrow |5, -3\rangle) - \nu(|4, -4\rangle \rightarrow |5, -4\rangle) = \frac{\mu_B g_5}{h} B, \quad (2)$$

where $\nu(|4, -4\rangle \rightarrow |5, -3\rangle)$ is the frequency of σ^+ -transition, $\nu(|4, -4\rangle \rightarrow |5, -4\rangle)$ – the frequency of π -transition, μ_B – the Bohr magneton, h – the Planck constant, g_5 – the Landefactor for $F = 5$ level.

The resulting experimentally obtained magnetic field profile is shown in Figure 3b. It has a pronounced maximum at the position of the main chamber coil and a local maximum at the position of the science chamber coil. The theoretical curve was rescaled along both axes to fit the experimental points.

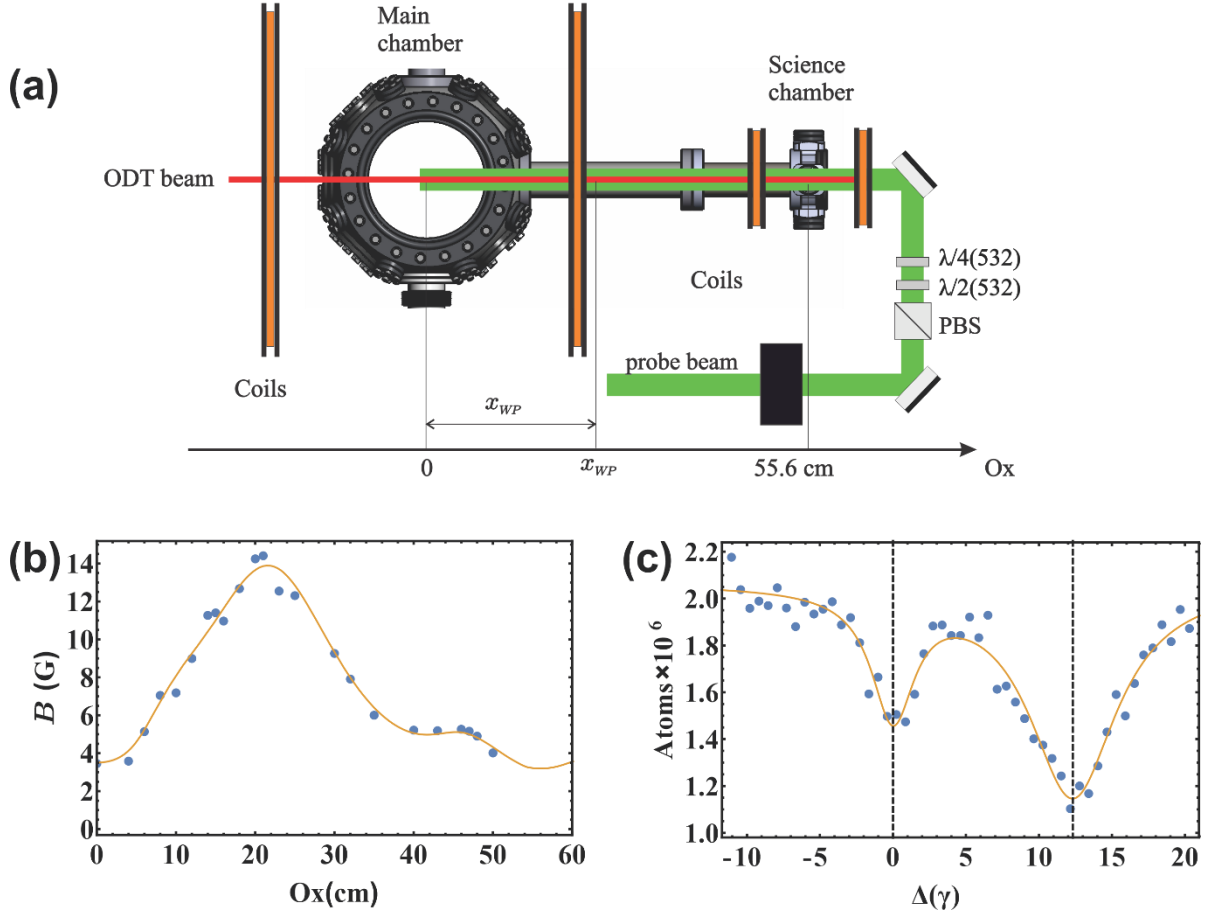


Figure 3. a) Setup of the magnetic field calibration experiment with optical resonance. b) Absolute value of the magnetic field along Ox at a current of 2 A in all coils. The red line is a fit of the experimental data with a rescaled theoretical curve. c) Typical optical resonances in the magnetic field calibration experiment. The plot is given in the number of atoms vs detuning from atomic resonance in units of γ .

IV. OPTICAL TRANSPORT

To perform the optical transport, the focus of the ODT beam is moved and the atoms are forced to follow the dipole force potential minimum. Given the dynamics of the position of the waist $x_{WP}(t)$, the dipole force along the Ox axis exerted on an atom with the coordinate x is determined by the potential

$$U(x, x_{WP}(t)) = - \frac{2\alpha P}{\pi (w_0(x_{WP}(t)))^2 \left(1 + \left(\frac{x_{WP}(t) - x}{x_{REL}} \right)^2 \right)}. \quad (3)$$

Here $w_0(x_{WP}(t))$ is the ODT beam waist depending on its position $x_{WP}(t)$ (see Figure 1), α – the polarizability of the thulium atom in the ODT, P – the total power of the ODT beam, x_{REL} – the Rayleigh length of the ODT beam. Experimentally, the $x_{WP}(t)$ is set via a focus-tunable lens using a preliminary measured calibration (Figure 1c).

In addition to dipole force, the magnetic field exerts a force on magnetic atoms depending on the gradient

$$\vec{F}_m = \nabla(\vec{\mu}\vec{B}) = \nabla(\mu \frac{\vec{B}}{B}) = \mu \nabla B, \quad (4)$$

where $\mu = m_F \mu_B g_5$ is the magnetic dipole moment of the atom. Note that the force depends only on the gradient of the magnetic field value because the magnetic moments of the atoms are aligned with the field.

The motion of the center of mass of a cloud of atoms along the Ox axis governed by Newton's second law was considered:

$$m\ddot{x}_{CM}(t) = F_{mx}(x_{CM}(t)) - \nabla U(x, x_{WP}(t))|_{x=x_{CM}(t)}, \quad (5)$$

where $x_{CM}(t)$ – the position of the center of mass of a cloud of atoms along the Ox axis. The projection of the magnetic force on the Ox axis can be calculated at $x_{CM}(t)$ using the previously obtained dependence of the magnetic field value.

An additional restriction was added for the field to be equal $B_0 = 3.8G$ at the $x_{CM}(t)$ to reduce losses of atoms from the trap. The value of the magnetic field can be factorized

$$B(x, t) = f(x)I(t) \text{ into the spatial part } f(x) \text{ and current } I(t). \text{ One can find } f(x) = \frac{B_{exp}(x)}{I_{exp}}$$

from experimentally measured values of the magnetic field $B_{exp}(x)$ along the Ox axis at the value of current $I_{exp} = 2A$. The desired current time dependence can be found from the relation

$$I(t) = \frac{B_0}{f(x_{CM}(t))} \text{ (see Figure 4a).}$$

The total duration of the transport has several restrictions. A bound from below is set by the characteristic time $T_0 = \nu_x^{-1}$, where ν_x is an ODT frequency along the transport axis: a very

fast ramp $T \ll T_0$ would be simply ignored by atoms and they would just leave the trap. A bound from above is set by the lifetime of atoms in the ODT measured not to exceed 6.3 s. Moreover, transferred atoms can oscillate after x_{WP} reaches the final value and stops in time.

The center of mass of a cloud of atoms was set up to move the distance l with a constant acceleration $|a_{CM}| = \frac{16l}{T^2}$, the first half accelerating and the last half decelerating [30]. The chosen value of acceleration determines the total time of transport and vice versa. Modeling results and test experiments led to the selection of $T = 20T_0$ to diminish the final oscillations of the atomic cloud. By solving equation (5), one can find the needed profile $x_{WP}(t)$ (see Figure 4b). It has a discontinuity (shown in a zoom in Figure 4b) at 1.684 s where a_{CM} has one. With this profile, the optical force would indeed compensate for the magnetic force during the entire transport (see Figure 4c). The desired trajectory $x_{CM}(t)$ and acceleration of a center of mass are presented in Figure 4d given $l = 55.6 \text{ cm}$ and $T = 3.168 \text{ s}$.

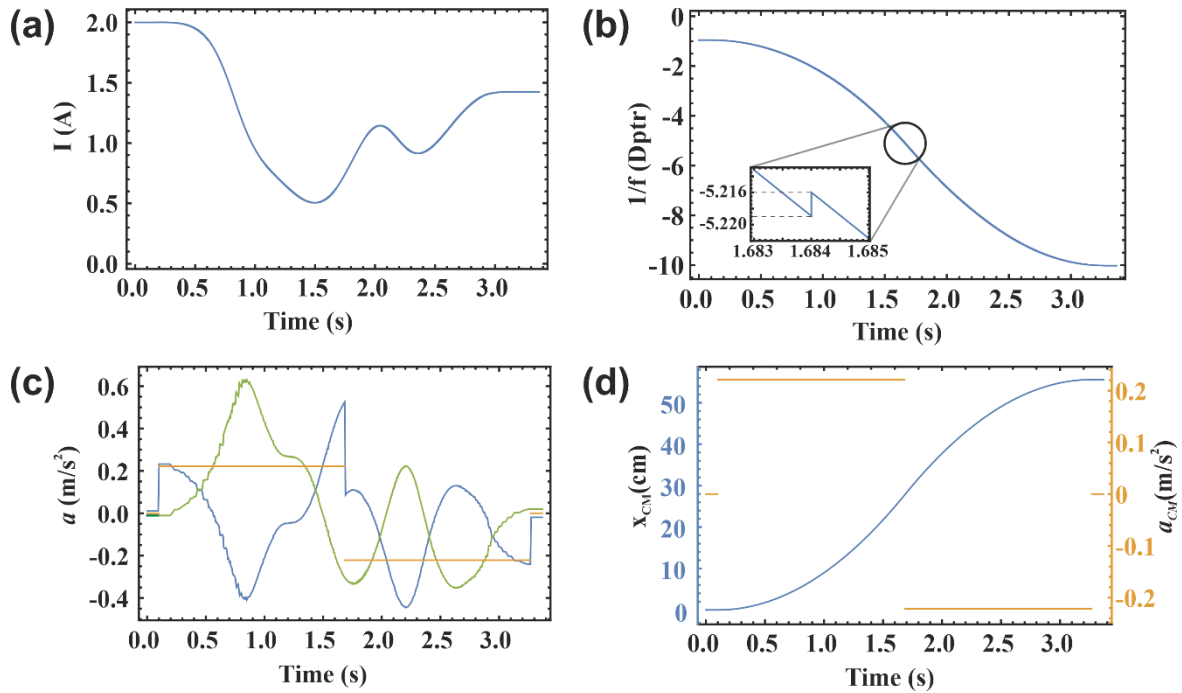


Figure 4. a) Modeled function of current in magnetic coils during optical transport. The amplitude of the magnetic field in the CM position is constant. b) Resulting optical power versus time. c) Acceleration of CM versus time (red line) and accelerations of CM from magnetic force (green line) and optical dipole force (blue

line) d) Model of CM motion. The blue line is a coordinate of CM of the cloud versus time, red line is an acceleration of CM of the cloud versus time.

The obtained $x_{wp}(t)$ function made it possible to transport $1.1 \cdot 10^6$ atoms to a distance of 55.6 cm. To estimate the efficiency of the transport, the number of atoms in the ODT was measured taking into account the trap depth reduction due to the beam waist change during transport (Figure 5a). The atoms after the transport revealed a slightly reduced temperature compared to those without transport (the depth changes and transport duration were considered, Figure 5b) – 21 versus 25 μK . The number of atoms in the ODT if stored for the same time, but transport was not implemented, was $3.2 \cdot 10^6$, thus a bit over 1/3 of the atoms were transported. Further improvement of this result is possible if higher aperture optics are used. Also, one can try to further improve the efficiency of transport with the machine learning approach [11,46].

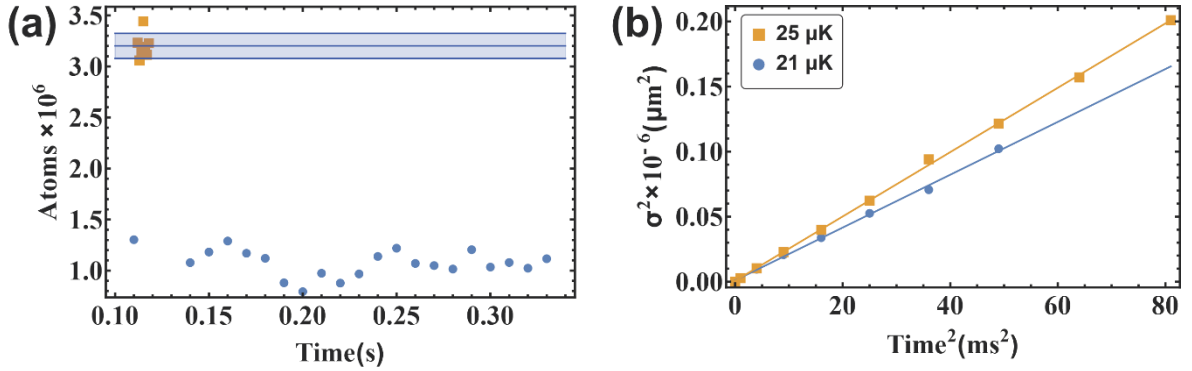


Figure 5. a) The number of atoms versus time after transport (blue dots) and without transport taking into account the depth changes during the transport (orange dots). The blue line is the mean number of atoms without transport with a standard deviation (blue area). b) Ballistic expansion of the atomic cloud after the transport (blue dots and blue line) and without transport taking into account depth changes during transport (orange dots and orange line).

V. CONCLUSION

In summary, the optical transport of magnetic thulium atoms was implemented. The calculation and measurement of the magnetic field along the transport made it possible to maintain it constant to reduce the losses related to the Fano-Feshbach resonance spectrum and to maintain the $|F = 4, m_F = -4\rangle$ state of atoms. The force of the magnetic field gradient was compensated

for by a sophisticated ramp for the lens with a tunable focus. As a result, $1.1 \cdot 10^6$ atoms were transported to a distance of 55.6 cm compared to $3.2 \cdot 10^6$ atoms remaining in the ODT without transport after the same period of storage time, as the time used for storage. The temperature was slightly reduced during transport compared to the case without one.

VI. ACKNOWLEDGMENTS

This work was supported by Rosatom in the framework of the Roadmap for Quantum computing (Contract No. 868-1.3-15/15-2021 dated October 5, 2021).

VII. REFERENCES

- [1] I. M. Georgescu, S. Ashhab, and F. Nori, Quantum simulation, *Rev Mod Phys* **86**, 153 (2014).
- [2] A. Trautmann, P. Ilzhöfer, G. Durastante, C. Politi, M. Sohmen, M. J. Mark, and F. Ferlaino, Dipolar Quantum Mixtures of Erbium and Dysprosium Atoms, *Phys Rev Lett* **121**, 213601 (2018).
- [3] M. Lu, N. Q. Burdick, and B. L. Lev, Quantum Degenerate Dipolar Fermi Gas, *Phys Rev Lett* **108**, 215301 (2012).
- [4] T. Lahaye, C. Menotti, L. Santos, M. Lewenstein, and T. Pfau, The physics of dipolar bosonic quantum gases, *Reports on Progress in Physics* **72**, 71 (2009).
- [5] S. Baier, D. Petter, J. H. Becher, A. Patscheider, G. Natale, L. Chomaz, M. J. Mark, and F. Ferlaino, Realization of a Strongly Interacting Fermi Gas of Dipolar Atoms, *Phys Rev Lett* **121**, 093602 (2018).
- [6] M. Lu, S. H. Youn, and B. L. Lev, Trapping ultracold dysprosium: A highly magnetic gas for dipolar physics, *Phys Rev Lett* **104**, 063001 (2010).
- [7] A. Petrov, E. Tiesinga, and S. Kotochigova, Anisotropy-induced Feshbach resonances in a quantum dipolar gas of highly magnetic atoms, *Phys Rev Lett* **109**, 103002 (2012).
- [8] G. Natale, T. Bland, S. Gschwendtner, L. Lafforgue, D. S. Grün, A. Patscheider, M. J. Mark, and F. Ferlaino, Bloch oscillations and matter-wave localization of a dipolar quantum gas in a one-dimensional lattice, *Communications Physics* 2022 5:1 **5**, 1 (2022).

- [9] A. J. Olson, D. L. Whitenack, and Y. P. Chen, Effects of magnetic dipole-dipole interactions in atomic Bose-Einstein condensates with tunable s-wave interactions, *Phys Rev A (Coll Park)* **88**, 043609 (2013).
- [10] J. Stuhler, A. Griesmaier, T. Koch, M. Fattori, T. Pfau, S. Giovanazzi, P. Pedri, and L. Santos, Observation of Dipole-Dipole Interaction in a Degenerate Quantum Gas, *Phys Rev Lett* **95**, 150406 (2005).
- [11] V. A. Khlebnikov, D. A. Pershin, V. V. Tsyganok, E. T. Davletov, I. S. Cojocaru, E. S. Fedorova, A. A. Buchachenko, and A. V. Akimov, Random to Chaotic Statistic Transformation in Low-Field Fano-Feshbach Resonances of Cold Thulium Atoms, *Phys Rev Lett* **123**, 213402 (2019).
- [12] V. A. Khlebnikov, V. V. Tsyganok, D. A. Pershin, E. T. Davletov, E. Kuznetsova, and A. V. Akimov, Characterizing the temperature dependence of Fano-Feshbach resonances of ultracold polarized thulium, *Phys Rev A (Coll Park)* **103**, 023306 (2021).
- [13] T. Maier et al., Emergence of Chaotic Scattering in Ultracold Er and Dy, *Phys Rev X* **5**, 041029 (2015).
- [14] A. Frisch et al., Ultracold Dipolar Molecules Composed of Strongly Magnetic Atoms, *Phys Rev Lett* **115**, 203201 (2015).
- [15] K. Baumann, N. Q. Burdick, M. Lu, and B. L. Lev, Observation of low-field Fano-Feshbach resonances in ultracold gases of dysprosium, *Phys Rev A (Coll Park)* **89**, 020701 (2014).
- [16] L. Tanzi, E. Lucioni, F. Famà, J. Catani, A. Fioretti, C. Gabbanini, R. N. Bisset, L. Santos, and G. Modugno, Observation of a Dipolar Quantum Gas with Metastable Supersolid Properties, *Phys Rev Lett* **122**, 130405 (2019).
- [17] L. Chomaz et al., Long-Lived and Transient Supersolid Behaviors in Dipolar Quantum Gases, *Phys Rev X* **9**, 021012 (2019).
- [18] M. Guo, F. Böttcher, J. Hertkorn, J. N. Schmidt, M. Wenzel, H. P. Büchler, T. Langen, and T. Pfau, The low-energy Goldstone mode in a trapped dipolar supersolid, *Nature* **574**, 386 (2019).
- [19] W. S. Bakr, J. I. Gillen, A. Peng, S. Fölling, and M. Greiner, A quantum gas microscope for detecting single atoms in a Hubbard-regime optical lattice, *Nature* **462**, 74 (2009).

- [20] L. W. Cheuk, M. A. Nichols, M. Okan, T. Gersdorf, V. v. Ramasesh, W. S. Bakr, T. Lompe, and M. W. Zwierlein, Quantum-Gas Microscope for Fermionic Atoms, *Phys Rev Lett* **114**, 193001 (2015).
- [21] S. Kuhr, Quantum-gas microscopes: A new tool for cold-atom quantum simulators, *Natl Sci Rev* **3**, 170 (2016).
- [22] E. Haller, J. Hudson, A. Kelly, D. A. Cotta, B. Peaudecerf, G. D. Bruce, and S. Kuhr, Single-atom imaging of fermions in a quantum-gas microscope, *Nat Phys* **11**, 738 (2015).
- [23] R. Yamamoto, J. Kobayashi, T. Kuno, K. Kato, and Y. Takahashi, An ytterbium quantum gas microscope with narrow-line laser cooling, *New J Phys* **18**, 023016 (2016).
- [24] R. Yamamoto, J. Kobayashi, K. Kato, T. Kuno, Y. Sakura, and Y. Takahashi, Site-resolved imaging of single atoms with a Faraday quantum gas microscope, *Phys Rev A (Coll Park)* **96**, 033610 (2017).
- [25] A. Browaeys and T. Lahaye, Many-body physics with individually controlled Rydberg atoms, *Nature Physics* 2020 16:2 **16**, 132 (2020).
- [26] A. Frisch, M. Mark, K. Aikawa, F. Ferlaino, J. L. Bohn, C. Makrides, A. Petrov, and S. Kotochigova, Quantum chaos in ultracold collisions of gas-phase erbium atoms, *Nature* **507**, 475 (2014).
- [27] H. J. Lewandowski, D. M. Harber, D. L. Whitaker, and E. A. Cornell, Observation of Anomalous Spin-State Segregation in a Trapped Ultracold Vapor, *Phys Rev Lett* **88**, 070403 (2002).
- [28] M. Greiner, I. Bloch, T. W. Hänsch, and T. Esslinger, Magnetic transport of trapped cold atoms over a large distance, *Phys Rev A (Coll Park)* **63**, 031401 (2001).
- [29] T. L. Gustavson, A. P. Chikkatur, A. E. Leanhardt, A. Görlitz, S. Gupta, D. E. Pritchard, and W. Ketterle, Transport of Bose-Einstein Condensates with Optical Tweezers, *Phys Rev Lett* **88**, 020401 (2001).
- [30] A. Couvert, T. Kawalec, G. Reinaudi, and D. Guéry-Odelin, Optimal transport of ultracold atoms in the non-adiabatic regime, *EPL (Europhysics Letters)* **83**, 13001 (2008).

- [31] J. Léonard, M. Lee, A. Morales, T. M. Karg, T. Esslinger, and T. Donner, Optical transport and manipulation of an ultracold atomic cloud using focus-tunable lenses, *New J Phys* **16**, 093028 (2014).
- [32] S. Schmid, G. Thalhammer, K. Winkler, F. Lang, and J. H. Denschlag, Long distance transport of ultracold atoms using a 1D optical lattice, *New J Phys* **8**, 159 (2006).
- [33] M. Miranda, R. Inoue, Y. Okuyama, A. Nakamoto, and M. Kozuma, Site-resolved imaging of ytterbium atoms in a two-dimensional optical lattice, *Phys Rev A (Coll Park)* **91**, 063414 (2015).
- [34] V. V Tsyganok et al., Polarized cold cloud of thulium atom, *Journal of Physics B: Atomic, Molecular and Optical Physics* **51**, 165001 (2018).
- [35] D. A. Pershin, V. V. Tsyganok, V. V. Yaroshenko, V. A. Khlebnikov, E. T. Davletov, E. L. Svechnikov, V. N. Sorokin, P. V. Kapitanova, and A. V. V. Akimov, Microwave Spectroscopy of Ultracold Thulium Atoms, *Bulletin of the Lebedev Physics Institute* **45**, 377 (2018).
- [36] V. V. V Tsyganok, D. A. A. Pershin, E. T. T. Davletov, V. A. A. Khlebnikov, and A. V. V Akimov, Scalar, tensor, and vector polarizability of Tm atoms in a 532-nm dipole trap, *Phys Rev A (Coll Park)* **100**, 042502 (2019).
- [37] V. V. Tsyganok et al., Losses of thulium atoms from optical dipole traps operating at 532 and 1064 nm, *Phys Rev A (Coll Park)* **107**, 023315 (2023).
- [38] V. V. Tsyganok et al., Bose-Einstein condensate as a diagnostic tool for an optical lattice formed by 1064-nm laser light, *Phys Rev A (Coll Park)* **108**, 013310 (2023).
- [39] E. T. Davletov, V. V. Tsyganok, V. A. Khlebnikov, D. A. Pershin, D. V. Shaykin, and A. V. Akimov, Machine learning for achieving Bose-Einstein condensation of thulium atoms, *Phys Rev A (Coll Park)* **102**, 011302 (2020).
- [40] A. Frisch, K. Aikawa, M. Mark, A. Rietzler, J. Schindler, E. Zupanič, R. Grimm, and F. Ferlaino, Narrow-line magneto-optical trap for erbium, *Phys Rev A (Coll Park)* **85**, 051401 (2012).
- [41] T. Maier, H. Kadau, M. Schmitt, A. Griesmaier, and T. Pfau, Narrow-line magneto-optical trap for dysprosium atoms, *Opt Lett* (2014).

- [42] T. H. Loftus, T. Ido, M. M. Boyd, A. D. Ludlow, and J. Ye, Narrow line cooling and momentum-space crystals, *Phys Rev A (Coll Park)* **70**, 063413 (2004).
- [43] B. Seo, P. Chen, Z. Chen, W. Yuan, M. Huang, S. Du, and G.-B. Jo, Efficient production of a narrow-line erbium magneto-optical trap with two-stage slowing, *Phys Rev A (Coll Park)* **102**, 013319 (2020).
- [44] E. Kalganova, O. Prudnikov, G. Vishnyakova, A. Golovizin, D. Tregubov, D. Sukachev, K. Khabarova, V. Sorokin, and N. Kolachevsky, Two-temperature momentum distribution in a thulium magneto-optical trap, *Phys Rev A (Coll Park)* **96**, 033418 (2017).
- [45] V. V. Tsyganok, D. A. Pershin, V. A. Khlebnikov, E. T. Davletov, and A. V. Akimov, Zeeman Spectroscopy of Ultracold Thulium Atoms, *Journal of Experimental and Theoretical Physics* **128**, (2019).
- [46] D. A. Kumpilov et al., Learning from machine learning: optimization of the Bose-Einstein condensate of the thulium atom at a 1064 trap, (2023).